Pergamon

Int. J. Solids Structures Vol. 32, No. 5, pp. 571–591, 1995

0020-7683/95 $9.50 + .00

0020-7683(94)00152-9

FINITE ELEMENT ANALYSIS OF ANISOTROPIC MATERIALS WITH SINGULAR INPLANE STRESS FIELDS

STEPHANE S. PAGEAU, PAUL F. JOSEPH
and SHERRILL B. BIGGERS JR†

Department of Mechanical Engineering, Clemson University, Clemson, SC 29634, U.S.A.

(*Received* 11 *March* 1994; *in revised form* 22 *June* 1994)

Abstract—A finite element formulation is developed for the analysis of singular stress states at material and geometric discontinuities in anisotropic materials loaded inplane. The displacement field of the sectorial element is quadratic in the angular coordinate direction and exponential in the radial direction measured from the singular point. The formulation of Yamada and Okumura (1983a, b) is extended to take into account the anisotropy of the material. The stress and displacement fields are obtained when the order of the stress singularity is real as well as complex. When the order of the stress singularity is complex, it is shown that the angular variation of the stress and displacement fields can be expressed in an infinite number of ways. Results for the displacement and stress fields obtained when the order of the stress singularity is complex can be made to match already published results once a similarity transformation is applied. The simplicity and accuracy of the formulation are demonstrated by comparison to several analytical solutions for both isotropic and anisotropic multi-material wedges and junctions with and without disbonds. The nature and rate of convergence associated with the element suggests that it could be used in developing enriched elements for use with standard elements to yield accurate and computationally efficient solutions to problems having complex global geometries.

INTRODUCTION

The finite element method is a well known and widely used method for determining stress intensity factors in linear elastic materials containing cracks. For instance, the ASTM standards for determining the fracture toughness of materials from test coupons make use of such an approach. The method requires the prior analytical knowledge of the nature of the singular stress field near the crack tip. Numerous authors, among them Bogy (1971), Hoenig (1982) and Sih *et al.* (1971), have helped establish this knowledge for cracked isotropic and anisotropic materials. These basic ideas of fracture mechanics can also be applied to failure initiation and crack growth at locations in structures where the stress fields are singular, not only due to the presence of cracks, but also due to material and/or geometrical discontinuities. A number of analytical solutions exist for the order of the singularity and for the angular variation of the stress and displacement fields around the singular point in multi-material wedges and junctions (Hein and Erdogan, 1971; Ma and Hour, 1989; Pageau *et al.*, 1994a). In combination with these solutions, the finite element method can be used to account for the specific far-field geometry and loading conditions and to evaluate the "stress intensity factors" associated with the singularity.

When analytical solutions are not available for a given type of material and/or geometrical discontinuity, the finite element method can be used directly to numerically establish the order of the stress singularities and the angular variation of stress and displacement fields in the vicinity of the singularity. The order of the stress singularity can be indirectly obtained from a finite element analysis using a direct curve fit on the stresses; see, for example, Raju and Crews (1981). More recently, Barsoum (1988a, b) and Sukumar and Kumosa (1992) have used a process called the finite element iterative method to obtain the converged order of the stress singularity. Gu and Belytschko (1994) use a spectral overlay method along with a least-square fit to obtain the order of the stress singularity. Among the authors who use a finite element eigenanalysis to determine the order of the stress

† Author to whom correspondence should be addressed.

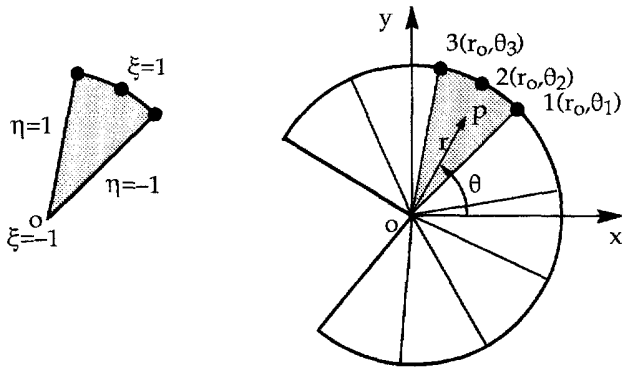

Fig. 1. Definition of the finite element geometry and natural coordinates in a typical structure where a singular stress state occurs.

singularity and the angular variation of the stress and displacement fields directly are Bazant and Estenssoro (1979) and Yamada and Okumura (1983a, b). In these last three papers, this eigenanalysis approach has also been used to evaluate the singularity at a point where a crack meets a free surface in an isotropic material. This solution agreed with the solution given by Benthem (1977) for a mode I loading of the crack. The recent paper by Gu and Belytschko (1994) also uses an eigenanalysis and compares results with their spectral overlay method.

The present paper adapts the inplane formulation developed by Yamada and Okumura (1983a, b) to inplane deformation of wedges and junctions composed of anisotropic materials. When the order of the stress singularity is real, obtaining the stress and displacement fields from this formulation is straightforward. This is not the case when the order of the stress singularity is complex, and therefore, this issue is addressed here in a separate section. The formulation is verified by comparison with existing analytical solutions for isotropic and anisotropic materials. Results for both the order of the stress singularities and the angular variation of the displacement and stress fields around singular locations are given. Finally, the method is applied to bonded and disbonded anisotropic bimaterial junctions in which singular stress states are present due to material and geometrical discontinuities. These examples demonstrate the simplicity and accuracy of the method.

FORMULATION

Finite element formulation for anisotropic materials

The formulation is directly extended from that of Yamada and Okumura (1983a) to account for anisotropic materials. Much of their formulation is summarized here in eqns (1)–(13) for completeness and for ease of application to anisotropic materials. Figure 1 presents a typical geometry where a singular stress state occurs at point o. The purpose of this formulation is to develop the methodology to determine the order of the stress singularity by means of a finite element study. For this purpose, the geometry is divided into several quadratic sector elements, with each element being located in polar coordinates by its nodes 1–3. A point P in the element can be located using the singular transformation of Yamada *et al.* (1979) by the relations

$$r = r_o\left(\frac{1+\xi}{2}\right)^{1/\lambda} \quad \text{or} \quad \rho = \frac{r}{r_o} = \left(\frac{1+\xi}{2}\right)^{1/\lambda} \tag{1}$$

$$\theta = \sum_{i=1}^{3} H_i\theta_i \tag{2}$$

where

$$H_1 = \tfrac{1}{2}(-\eta+\eta^2), \quad H_2 = 1-\eta^2, \quad H_3 = \tfrac{1}{2}(\eta+\eta^2), \tag{3}$$

and η and ξ are natural coordinates of the element whose ranges are defined as shown in Fig. 1.

The displacement field in the element subjected to inplane loads is assumed to be of the form

$$(u-u_o) = \left(\frac{1+\xi}{2}\right)\left[\sum_{i=1}^{3} H_i\,(u_i-u_o)\right] \tag{4}$$

where u_o and u represent the inplane-displacement vector of the vertex o and the point P, respectively, and u_i represents the inplane-displacement vector of the node i ($i = 1, 2, 3$).

In order to simplify the notation and to measure displacements relative to that of the vertex o, we define $\bar{u}_i = (u_i-u_o)$ and $\bar{u} = (u-u_o)$. Using eqn (1), eqn (4) can be written with the new notation as

$$\bar{u} = \rho^{\lambda}\left[\sum_{i=1}^{3} H_i\bar{u}_i\right]. \tag{5}$$

The strains are then obtained directly from eqns (1)–(3), and (5) as

$$\{\varepsilon\} = \begin{Bmatrix} \varepsilon_r \\ \varepsilon_\theta \\ \gamma_{r\theta} \end{Bmatrix} = \sum_{i=1}^{3} [B_i]\{\bar{u}_i\} = [B]\{\bar{u}\}, \quad \{\bar{u}_i\} = \begin{Bmatrix} \bar{u}_{ri} \\ \bar{u}_{\theta i} \end{Bmatrix} \tag{6}$$

where

$$[B] = \frac{1}{r_o}\rho^{\lambda-1}(\lambda[B_a]+[B_b]), \quad [B_{ia}] = \begin{bmatrix} H_i & 0 \\ 0 & 0 \\ 0 & H_i \end{bmatrix},$$

$$[B_{ib}] = \begin{bmatrix} 0 & 0 \\ H_i & \dfrac{2}{\theta_s}\dfrac{\partial H_i}{\partial \eta} \\ \dfrac{2}{\theta_s}\dfrac{\partial H_i}{\partial \eta} & -H_i \end{bmatrix}, \quad i = 1,2,3. \tag{7}$$

It has been assumed that $\theta_2 = (\theta_1+\theta_3)/2, \theta_s = \theta_3-\theta_1$, and therefore $\partial\eta/\partial\theta = 2/\theta_s$.

Equations (6) and (7) show that the strains and therefore the stresses are proportional to $\rho^{\lambda-1}$. The case where $0 < \mathrm{Re}(\lambda) < 1$ defines a singular stress state at the vertex o of the element. Application of the principal of virtual work leads to the following characteristic equation, for the entire domain S defined in Fig. 1:

$$(\lambda^2[A]+\lambda[B]+[C])\{\bar{U}\} = 0, \tag{8}$$

where

$$[A] = \sum_S([k_a]-[k_{sa}]), \quad [B] = \sum_S([k_b]-[k_{sb}]), \quad [C] = \sum_S[k_c], \quad \{\bar{U}\} = \sum_S\{\bar{u}\} \tag{9}$$

$$[k_a] = \int_{-1}^{1} [B_a]^T[D][B_a]\,\mathrm{d}\eta \tag{10}$$

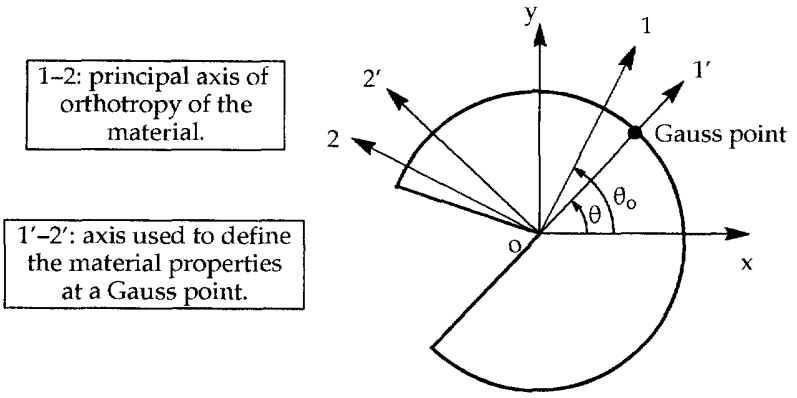

Fig. 2. Reference axis systems for determining local mechanical properties.

$$[k_c] = \int_{-1}^{1} [B_b]^{\mathrm{T}}[D][B_b]\,\mathrm{d}\eta \tag{11}$$

$$[k_b] = \int_{-1}^{1} ([B_a]^T[D][B_b] + [B_b]^T[D][B_a])\,\mathrm{d}\eta \tag{12}$$

$$[k_{sa}] = 2\int_{-1}^{1} [H]^T[d][B_a]\,\mathrm{d}\eta\,, \quad [k_{sb}] = 2\int_{-1}^{1} [H]^T[d][B_b]\,\mathrm{d}\eta \tag{13}$$

and where the summation over S implies assembly of the elements into the global model. The characteristic eqn (8) can be transformed into a standard eigenvalue problem,

$$[S]\begin{Bmatrix}\bar{V}\\ \bar{U}\end{Bmatrix} = \lambda\begin{Bmatrix}\bar{V}\\ \bar{U}\end{Bmatrix}, \quad [S] = \begin{bmatrix}0 & I\\ -A^{-1}C & -A^{-1}B\end{bmatrix}. \tag{14}$$

The element matrices $[k]$ are evaluated using numerical integration by means of Gaussian quadrature. The material stiffness matrix $[D]$ applies to anisotropic materials whose properties are symmetric with respect to the $z = 0$ plane (monoclinic material), for which the inplane behavior of a structure clearly decouples from the antiplane behavior. $[D]$ must be evaluated at each Gauss point during the numerical evaluation of the integrals, such that the anisotropy in the material is correctly taken into consideration. Figure 2 depicts a monoclinic material whose principal axes of orthotropy are defined by the axis 1–2, at an angle of θ_o with respect to the global x–y axis. The properties of this material at the Gauss point shown in the figure, which has polar axis 1′–2′ forming an angle of θ with respect to the global axis x–y, are defined as

$$[D] = \begin{bmatrix}D_{11} & D_{12} & D_{16}\\ D_{12} & D_{22} & D_{26}\\ D_{16} & D_{26} & D_{66}\end{bmatrix}, \tag{15}$$

where

$$D_{11} = \frac{p_1\cos^4(\theta_1) + p_2\sin^4(\theta_1) + 2\cos^2(\theta_1)\sin^2(\theta_1)(2G_{12}p_3 + p_4)}{p_3}, \tag{16}$$

$$D_{12} = \frac{p_4(\cos^4(\theta_1) + \sin^4(\theta_1)) + \cos^2(\theta_1)\sin^2(\theta_1)(p_1 + p_2 - 4G_{12}p_3)}{p_3}, \tag{17}$$

$$D_{16} = \cos(\theta_1)\sin(\theta_1)\frac{p_1\cos^2(\theta_1) - p_2\sin^2(\theta_1) + (\sin^2(\theta_1) - \cos^2(\theta_1))(2G_{12}p_3 + p_4)}{p_3}, \tag{18}$$

$$D_{22} = \frac{p_2\cos^4(\theta_1) + p_1\sin^4(\theta_1) + 2\cos^2(\theta_1)\sin^2(\theta_1)(2G_{12}p_3 + p_4)}{p_3}, \tag{19}$$

$$D_{26} = \cos(\theta_1)\sin(\theta_1)\frac{p_1\sin^2(\theta_1) - p_2\cos^2(\theta_1) - (\sin^2(\theta_1) - \cos^2(\theta_1))(2G_{12}p_3 + p_4)}{p_3}, \tag{20}$$

$$D_{66} = \frac{G_{12}p_3(1 - 4\cos^2(\theta_1)\sin^2(\theta_1)) + \sin^2(\theta_1)\cos^2(\theta_1)(p_1 + p_2 - 2p_4)}{p_3}, \tag{21}$$

and where

$$p_1 = -E_1^2, \quad p_2 = -E_1E_2, \quad p_3 = \upsilon_{12}^2E_2 - E_1, \quad p_4 = -\nu_{12}E_1E_2, \tag{22}$$

for plane stress,

$$\begin{aligned} p_1 &= E_1^2(E_3\nu_{23}^2 - E_2), \quad p_2 = E_2^2(E_3\nu_{13}^2 - E_1), \\ p_3 &= \nu_{13}^2E_2E_3 + 2\nu_{23}\nu_{13}\nu_{12}E_2E_3 + \nu_{12}^2E_2^2 + \nu_{23}^2E_1E_3 - E_1E_2 \\ p_4 &= -E_1E_2(\nu_{12}E_2 + \nu_{23}\nu_{13}E_3), \end{aligned} \tag{23}$$

for plane strain, and

$$\theta_1 = \theta_0 - \theta. \tag{24}$$

The quantities $E_1, E_2, E_3, \nu_{12}, \nu_{13}, \nu_{23}$, and G_{12} are the mechanical properties of the material in the coordinate system 1–2. The first and last rows of $[D]$ in eqn (15) comprise matrix $[d]$. The trigonometric functions involved in $[D]$ and $[d]$ do not permit an exact integration using Gauss quadrature, unless the material is isotropic. For the isotropic case, exact integration can be performed using three Gauss quadrature points per element. The influence of the number of integration points used in computing the elements in eqn (14) will be described in a later section.

Obtaining the displacement field from the formulation

When the eigenvalue λ obtained from eqn (14) is real, the eigenvector $\bar{U}$ defines the relative inplane displacements at the nodes of the elements, that is, at $r = r_0$ for this element. Since these relative displacements are the same, except for a constant, at all r, the eigenvector can be viewed as the angular variation of the displacements on rays from the apex through the nodes. The angular variation of the displacements on rays between nodes can be obtained by curve fit, or by use of the shape functions. It is convenient to normalize the eigenvector such that the largest component is 1.0 in absolute value. The complete displacement field can be written in standard form as:

$$u_j = k\left(\frac{r}{r_0}\right)^{\lambda}(A_j), \quad j = 1, 2 \tag{25}$$

where $u_1 = u_r$ and $u_2 = u_\theta$ represent the radial and tangential displacements, respectively, and A_1 and A_2 represent the angular variation of the radial and tangential displacements,

respectively. k is a constant or "generalized stress intensity factor", which depends on the given loading and global geometry of the structure. The A_j, $j = 1, 2$, are obtained from the eigenvector at the nodes and by curve fit or by means of the shape functions at angles which do not correspond to the location of a node.

When the eigenvalue λ is complex, the meaning of the eigenvector, also complex, requires a more detailed explanation. In generic form the inplane displacements can be written as

$$u_j = k\left(\frac{r}{r_0}\right)^{\mathrm{Re}(\lambda)+\mathrm{i}\mathrm{Im}(\lambda)}(A_j+\mathrm{i}B_j), \quad j = 1,2, \quad \mathrm{i}^2 = -1 \tag{26}$$

where $u_1 = u_r$ and $u_2 = u_\theta$ represent the radial and tangential displacement, respectively, and A_1, B_1, and A_2, B_2 represent the angular variation of the radial and tangential displacement, respectively. A_j and B_j are obtained from the eigenvector at the nodes and are obtained by curve fit or by means of the shape functions at angles which do not correspond to the location of a node.

In real form, eqn (26) becomes

$$u_j = \left(\frac{r}{r_0}\right)^{\beta}\left[k_1\left\{A_j\cos\left(\varepsilon\ln\left(\frac{r}{r_0}\right)\right)-B_j\sin\left(\varepsilon\ln\left(\frac{r}{r_0}\right)\right)\right\}\right.$$
$$\left.+k_2\left\{A_j\sin\left(\varepsilon\ln\left(\frac{r}{r_0}\right)\right)+B_j\cos\left(\varepsilon\ln\left(\frac{r}{r_0}\right)\right)\right\}\right], \quad j = 1,2 \tag{27}$$

where $\beta = \mathrm{Re}(\lambda)$, $\varepsilon = \mathrm{Im}(\lambda)$, and k_1 and k_2 are constants which can be determined by the geometry and loading conditions for a given problem which contains a singularity of the type investigated in this study. Equation (27) can easily be rewritten as

$$u_j = (r)^{\beta}[k_1'\{A_j\cos(\varepsilon\ln(r))-B_j\sin(\varepsilon\ln(r))\}+k_2'\{A_j\sin(\varepsilon\ln(r))+B_j\cos(\varepsilon\ln(r))\}], \tag{28}$$

where

$$k_1' = \left(\frac{1}{r_0}\right)^{\beta}\{k_1\cos(\varepsilon\ln(r_0))-k_2\sin(\varepsilon\ln(r_0))\},$$

$$k_2' = \left(\frac{1}{r_0}\right)^{\beta}\{k_1\sin(\varepsilon\ln(r_0))+k_2\cos(\varepsilon\ln(r_0))\}, \quad j = 1,2.$$

Equation (28) shows that the angular variation of the displacements represented by the eigenvector $A_j+\mathrm{i}B_j$, is independent of the size of the finite elements, r_0. Note that the constants in eqn (28) are just transformed from the original solution developed in eqn (27).

It may be convenient here again to normalize the eigenvector which is produced by a given eigenvalue routine as the complex number $(A_j+\mathrm{i}B_j)$. Normalizing a complex number typically means multiplying that number by another complex number. In real form where A_j and B_j can be seen as the plane components of a vector, this normalization process is the same as transformation of A_j and B_j by a similarity transformation. Defining

$$A_j' = \phi(A_j\cos(\theta)-B_j\sin(\theta)) \tag{29}$$

$$B_j' = \phi(A_j\sin(\theta)+B_j\cos(\theta)) \tag{30}$$

where A_j' and B_j' represent another normalized eigenvector obtained after application of

the similarity transformation of magnification factor ϕ and rotation angle θ, eqn (28) becomes

$$u_j = (r)^{\beta}[k_1''\{A_j'\cos(\varepsilon\ln(r)) - B_j'\sin(\varepsilon\ln(r))\} + k_2''\{A_j'\sin(\varepsilon\ln(r)) + B_j'\cos(\varepsilon\ln(r))\}], \quad (31)$$

where

$$k_1'' = \frac{1}{\phi}(k_1'\cos(\theta) - k_2'\sin(\theta)), \quad (32)$$

$$k_2'' = \frac{1}{\phi}(k_1'\sin(\theta) + k_2'\cos(\theta)), j = 1, 2. \quad (33)$$

Equations (28) and (31) can appear to be very different, depending on the normalization scheme chosen for the eigenvector. However, eqns (28) and (31) are equivalent. There exists an angle θ and a magnification factor ϕ through which one of the eigenvectors can be transformed to bring it to agreement with the other eigenvector, that is, through eqns (29) and (30). The existence of apparently different, but equivalent, complex eigenvectors was observed by Barsoum (1988b) as an acceptable "non-convergence" of the eigenvectors during the iterative process used there.

It is interesting to note how the coefficients k_1' and k_2', which are a function of the geometry and the loading conditions, also depend on which eigenvector was chosen to write eqn (28) or (31). The fact that eigenvectors normalized in all possible ways can be obtained from one another by a similarity transformation as defined by eqns (29) and (30) also implies that the coefficients of the problem can be obtained by a similarity transformation whose magnification factor and rotation angle are as defined by eqns (32) and (33). The value $\sqrt{k_1''^2 + k_2''^2}$ is an invariant with respect to rotation as seen from eqns (32) and (33). Due to the multiplicity of the possible solutions for k_1'' and k_2'', these coefficients do not have any significant physical meaning when they are considered individually. Only the combined quantity $\sqrt{k_1''^2 + k_2''^2}$ has a value of physical significance. For example, it has been shown for a bimaterial crack problem by Lin and Mar (1979) that the latter value can be directly related to the strain energy release rate of the structure.

Obtaining the strain and stress fields from the formulation

When the eigenvalue λ obtained from eqn (14) is real, there is no problem obtaining the angular variation of the strains by making use of eqns (6) and (7) since the nodal values of inplane displacements are extracted from the eigenvector obtained after solving eqn (14), as previously explained. The stresses can be obtained directly from the strains by making use of the constitutive relation $\{\sigma\} = [D]\{\varepsilon\}$.

When the eigenvalue λ is complex, using eqns (6) and (7) is not straightforward. A way to avoid the difficulty of having complex numbers in these equations is to start from eqn (28) or (31) and differentiate with respect to r and θ to obtain the strains. Differentiation with respect to r can be performed analytically and does not present any difficulty. Differentiation with respect to θ can only be done numerically element by element using the derivatives of the shape functions H_i according to the relation $\partial H_i/\partial\theta = (2/\theta_s)(\partial H_i/\partial\eta)$. The stresses are obtained from the strains as indicated above.

RESULTS

Convergence of the finite element code

Isotropic materials. As stated earlier, exact integration of the eqns (9)–(13) is achieved with numerical integration using three Gauss points per element. The question then arises as to the number of elements needed to achieve sufficient accuracy in the evaluations of the

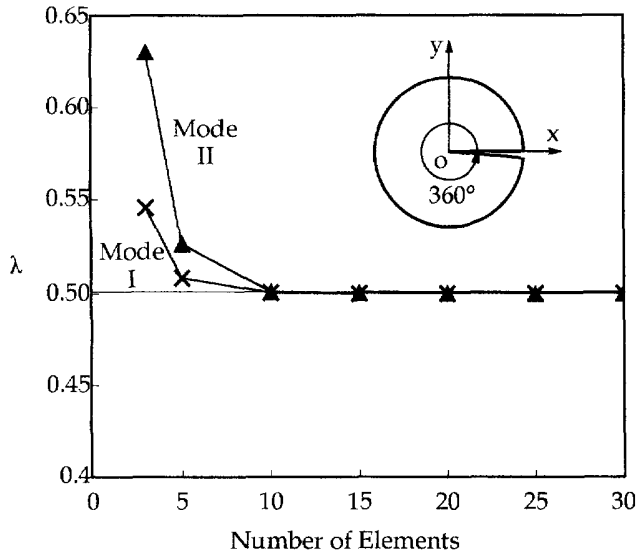

Fig. 3. Convergence of λ for a single isotropic material with a crack (mode I and mode II).

root λ obtained from eqn (14). The well-known single-material crack problem shown in Fig. 3 is the first test case used to evaluate convergence. The exact value of λ for this problem is 0.5 for both mode I and mode II deformation. The values of λ predicted by the finite element method using eqn (14) are shown in Fig. 3 and in Table 1 as a function of the number of equal-sized elements composing the 2π wedge angle. These data show a very strong, monotonic convergence toward the exact solution. The values of λ for mode I converge slightly faster than those for mode II. Note that no use of symmetry has been made in computing the results shown in Table 1. The same values for λ could be obtained for each mode with half as many elements if symmetry is accounted for in the model. This simple case offers promise that convergence may also be excellent when more than one material is present both for bonded and disbonded junctions. A later section will show the convergence trend for these more complicated cases in comparison with the exact solutions.

Anisotropic materials. Gaussian quadrature does not integrate the element stiffness matrices exactly when the material is anisotropic since the local material properties are not constant over the element. This adds to the problem of convergence associated with element size discussed in the previous section. The single material crack problem is used here again as a test case but with anisotropic (monoclinic) material properties as shown in Fig. 4. The exact solution for λ is again 0.5 as indicated by Sih *et al.* (1965). The results from eqn (14)

Table 1. Values of λ for an isotropic material with a crack (Fig. 3)

No. elements in model	Mode I	Mode II
3	0.545641	0.630267
5	0.508455	0.526639
10	0.500654	0.501963
15	0.500134	0.500401
20	0.500043	0.500129
25	0.500018	0.500053
30	0.500009	0.500026

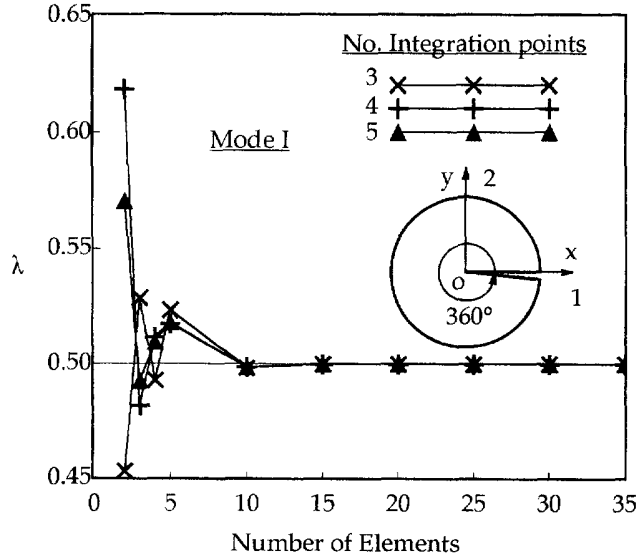

Fig. 4. Convergence of λ for a single anisotropic material with a crack (mode I).

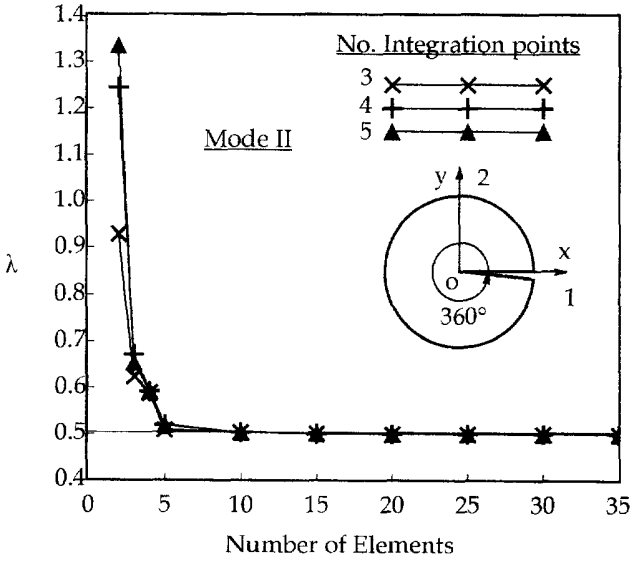

Fig. 5. Convergence of λ for a single anisotropic material with a crack (mode II).

are presented in Figs 4 and 5, and in Table 2. Integration with 3, 4, and 5 Gauss points per element was used for models with various degrees of mesh refinement. When only a very few elements are used, no clear trend is evident between accuracy and the number of Gauss points. With models large enough to yield values of λ accurate to within 1%, the integration scheme does not significantly affect the results. Therefore, for computational efficiency, the results to be presented in the remainder of the paper were obtained using three integration points per element. The major difference between the results for the isotropic and anisotropic materials is that in the latter case, convergence is oscillatory for mode I, as shown in Fig. 4, and convergence is not as rapid as in the isotropic case. This oscillatory convergence has also been observed for the antiplane shear case (Pageau *et al.*, 1994b). However, the difference between the convergence trends for isotropic and anisotropic materials observed there for antiplane shear is not as large as observed in the current case. This is due to the simplification in the formulation which is possible for antiplane shear of isotropic materials [i.e. eqns (25)–(28) in Pageau *et al.* (1994b)] and is not possible for the inplane case.

Table 2. Values of λ for an anisotropic material with a crack (Figs 4 and 5)

No. elements in model	Mode I			Mode II		
	3 Gauss points	4 Gauss points	5 Gauss points	3 Gauss points	4 Gauss points	5 Gauss points
2	0.453191	0.618349	0.570665	0.928725	1.244502	1.335052
3	0.528741	0.482038	0.492669	0.624371	0.672879	0.653897
4	0.493052	0.511723	0.509676	0.588732	0.592844	0.593194
5	0.523579	0.517739	0.518098	0.509105	0.520047	0.519757
10	0.498454	0.498773	0.498767	0.503876	0.503667	0.503673
15	0.500019	0.500021	0.500021	0.500987	0.500988	0.500988
20	0.500026	0.500026	0.500026	0.500308	0.500308	0.500308
25	0.500004	0.500004	0.500004	0.500136	0.500136	0.500136
30	0.500002	0.500002	0.500002	0.500067	0.500067	0.500067
35	0.500001	0.500001	0.500001	0.500037	0.500037	0.500037

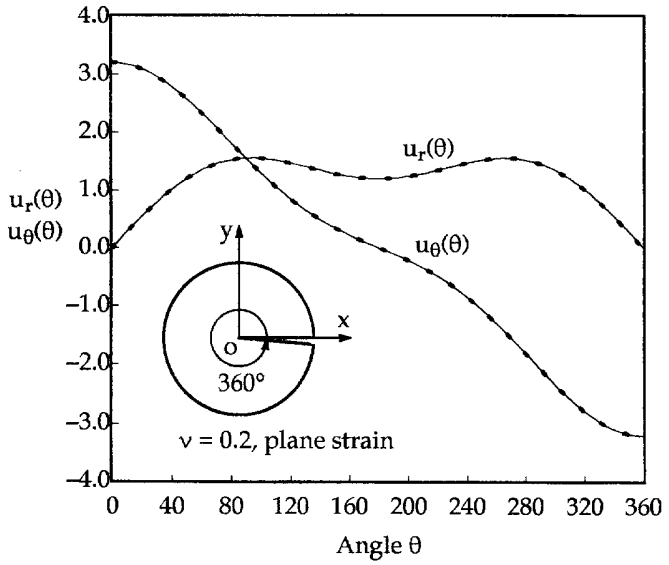

Fig. 6. Displacement field for a mode I loading of the crack. Analytical and FEM (10-element model) solutions are concident (dashed line = analytical solution).

Comparison of the finite element displacement field with analytical solutions

Real eigenvalue λ. The isotropic material with a crack as shown in Fig. 3 is used as the first test case. The angular variation of the radial and tangential displacements are obtained as explained above from eqn (25). Unlike the eigenvalue λ which determines the order of the stress singularity in r, the angular variation depends on the Poisson's ratio ν, and the type of planar loading. The results obtained for modes I and II from the current formulation are plotted against the well-known exact solutions for this problem, as shown in Figs 6 and 7. In this case a value of $\nu = 0.2$ is used and the finite element model contains 10 quadratic elements. Despite some inaccuracy in λ (0.13 and 0.39% error for mode I and mode II, respectively) the displacements are in excellent agreement with the exact solution. Additional elements in the model would improve the accuracy in both λ and displacements and might be needed if stresses and strains are required. An investigation of the effect of the number of elements needed to obtain converged strains and stresses is shown by Pageau *et al.* (1994b) for the antiplane case. The same trends observed there apply to the present inplane problem.

Complex eigenvalue λ. The test case investigated is that of a bimaterial crack problem as shown in Fig. 8. An exact solution derived by Chen (1985) is repeated here using the same notation as follows:

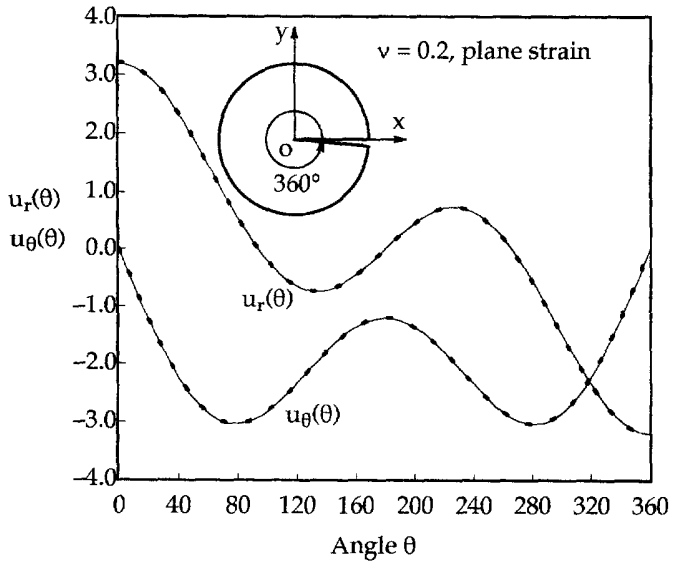

Fig. 7. Displacement field for a mode II loading of the crack. Analytical and FEM (10-element model) solutions are concident (dashed line = analytical solution).

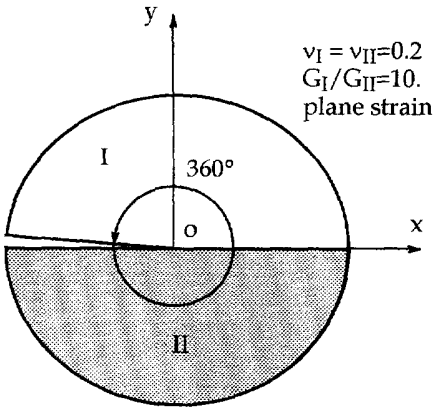

Fig. 8. Geometry of a bimaterial crack problem.

$$u_j = \sqrt{\frac{r}{2\pi}}\frac{1}{4G_j}[K_I(D_j + 2\delta_j \sin(\theta)\sin(\Theta)) - K_{II}(E_j - 2\delta_j \sin(\theta)\cos(\Theta))], \tag{34}$$

$$v_j = \sqrt{\frac{r}{2\pi}}\frac{1}{4G_j}[-K_I(E_j + 2\delta_j \sin(\theta)\cos(\Theta)) - K_{II}(D_j - 2\delta_j \sin(\theta)\sin(\Theta))], \tag{35}$$

where

$$\delta_1 = e^{-(\pi-\theta)\varepsilon}, \tag{36}$$

$$\delta_2 = e^{(\pi+\theta)\varepsilon}, \tag{37}$$

$$\Theta = \varepsilon \ln(r) + \frac{\theta}{2}, \tag{38}$$

$$D_j = \beta\gamma_j \cos\left(\frac{\theta}{2}\right) + \beta'\gamma'_j \sin\left(\frac{\theta}{2}\right), \tag{39}$$

$$E_j = \beta'\gamma_j \cos\left(\frac{\theta}{2}\right) - \beta\gamma_j' \sin\left(\frac{\theta}{2}\right), \tag{40}$$

$$\beta = \frac{0.5\cos(\varepsilon \ln(r)) + \varepsilon \sin(\varepsilon \ln(r))}{0.25+\varepsilon^2}, \tag{41}$$

$$\beta' = \frac{0.5\sin(\varepsilon \ln(r)) - \varepsilon \cos(\varepsilon \ln(r))}{0.25+\varepsilon^2}, \tag{42}$$

$$\gamma_j = \kappa_j\delta_j - \frac{1}{\delta_j}, \tag{43}$$

$$\gamma_j' = \kappa_j\delta_j + \frac{1}{\delta_j}, \tag{44}$$

$$2\pi\varepsilon = \ln\left[\frac{\frac{\kappa_1}{G_1}+\frac{1}{G_2}}{\frac{\kappa_2}{G_2}+\frac{1}{G_1}}\right], \quad j = 1,2, \quad -180 < \theta < 180. \tag{45}$$

The variables κ_j, G_j, u_j, v_j are the Kolosov constant, the shear modulus in material j, and the x and y displacements in material j, respectively. The eqns (34) and (35) can be easily rewritten as

$$u_j = \sqrt{\frac{r}{2\pi}}\frac{1}{4}[K_I(f_j(\theta)\cos(\varepsilon \ln(r)) - g_j(\theta)\sin(\varepsilon \ln(r))) - K_{II}(f_j(\theta)\sin(\varepsilon \ln(r)) + g_j(\theta)\cos(\varepsilon \ln(r)))], \tag{46}$$

$$v_j = \sqrt{\frac{r}{2\pi}}\frac{1}{4}[K_I(h_j(\theta)\cos(\varepsilon \ln(r)) - l_j(\theta)\sin(\varepsilon \ln(r))) - K_{II}(h_j(\theta)\sin(\varepsilon \ln(r)) + l_j(\theta)\cos(\varepsilon \ln(r)))], \tag{47}$$

where

$$f_j(\theta) = \frac{D_j(r=1) + 2\delta_j \sin(\theta)\sin(\Theta(r=1))}{G_j}, \tag{48}$$

$$g_j(\theta) = \frac{E_j(r=1) - 2\delta_j \sin(\theta)\cos(\Theta(r=1))}{G_j}, \tag{49}$$

$$h_j(\theta) = -\frac{E_j(r=1) + 2\delta_j \sin(\theta)\cos(\Theta(r=1))}{G_j}, \tag{50}$$

$$l_j(\theta) = \frac{D_j(r=1) - 2\delta_j \sin(\theta)\sin(\Theta(r=1))}{G_j}, \tag{51}$$

and the expression $D_j(r=1)$ means that D_j is evaluated at $r=1$. The functions f_j, g_j, h_j, and l_j are functions of the angle θ only, in view of eqns (38)–(42). The eqns (46) and (47) are comparable to eqn (28). Note that the subscript "j" in eqn (28) is utilized to distinguish the radial from the tangential displacement, whereas here, the subscript "j" is used to distinguish the two materials. The form of the eqns (46) and (47) remains unchanged if the displacements are expressed in polar form instead of Cartesian form. They become

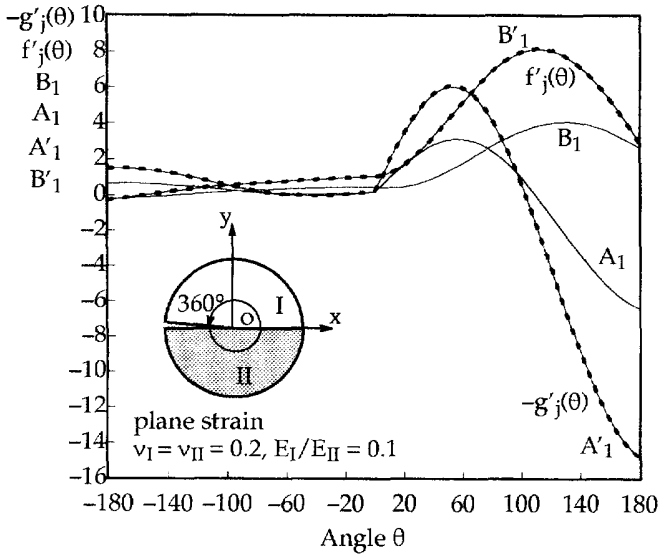

Fig. 9. Radial displacement field for a bimaterial crack. Analytical and FEM (10-element model) solutions are coincident after normalization (dashed line = analytical solution).

$$u_{rj} = \sqrt{\frac{r}{2\pi}}\frac{1}{4}[K_I(f'_j(\theta)\cos(\varepsilon \ln(r)) - g'_j(\theta)\sin(\varepsilon \ln(r))) - K_{II}(f'_j(\theta)\sin(\varepsilon \ln(r)) + g'_j(\theta)\cos(\varepsilon \ln(r)))], \quad (52)$$

$$u_{\theta j} = \sqrt{\frac{r}{2\pi}}\frac{1}{4}[K_I(h'_j(\theta)\cos(\varepsilon \ln(r)) - l'_j(\theta)\sin(\varepsilon \ln(r))) - K_{II}(h'_j(\theta)\sin(\varepsilon \ln(r)) + l'_j(\theta)\cos(\varepsilon \ln(r)))], \quad (53)$$

where,

$$f'_j(\theta) = f_j(\theta)\cos(\theta) + h_j(\theta)\sin(\theta), \quad (54)$$

$$g'_j(\theta) = g_j(\theta)\cos(\theta) + l_j(\theta)\sin(\theta), \quad (55)$$

$$h'_j(\theta) = -f_j(\theta)\sin(\theta) + h_j(\theta)\cos(\theta), \quad (56)$$

$$l'_j(\theta) = -g_j(\theta)\sin(\theta) + l_j(\theta)\cos(\theta). \quad (57)$$

Since eqns (52) and (53) are of the same form as eqn (28), only the angular functions f'_j, g'_j, h'_j, and l'_j, need to be compared to those obtained from the finite element formulation. The functions f'_j and g'_j can be compared to the angular functions A_1 and B_1 obtained from the finite element formulation for the radial displacement u_1. In the same way, the functions h'_j and l'_j are comparable to the angular functions A_2 and B_2 obtained for the tangential displacement u_2. Note that the angular functions A_1, B_1, A_2 and B_2 are obtained from the complex eigenvector at the nodes and by means of the shape functions between nodes.

The finite element and exact angular functions are shown in Figs 9 and 10. The exact value of the order of the stress singularity for the material properties chosen is $0.500000 + 0.100913i$. With only 10 elements chosen to model the entire wedge, the value of the order of the stress singularity is $0.501291 + 0.101173i$. Figure 9 provides the exact solution of Chen (1985) for $f'_j(\theta)$ and $-g'_j(\theta)$, in dashed lines. The solution for the eigenvector $(A_1 + iB_1)$ obtained directly from the finite element solution (after application of a magnification factor of 20 in order to clarify the figure) is also plotted in solid lines. A_1 and B_1 differ in amplitude and phase from Chen's (1985) analytical solution, and therefore

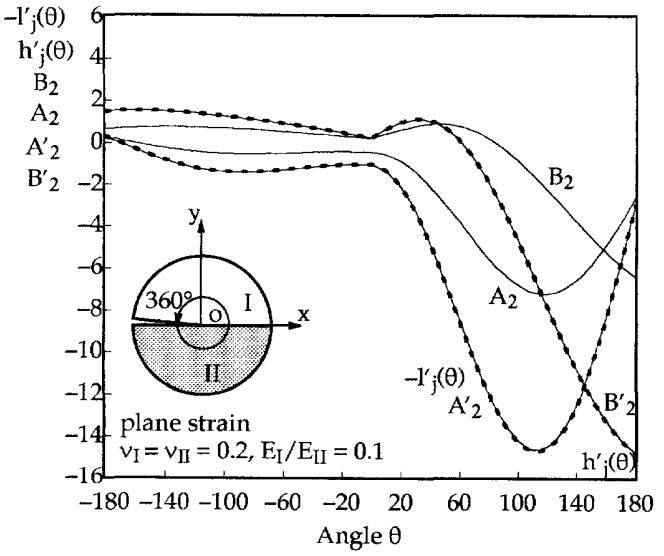

Fig. 10. Tangential displacement field for a bimaterial crack. Analytical and FEM (10-element model) solutions are coincident after normalization (dashed line = analytical solution).

appear different. However, the finite element solution is correct. This solution can be compared to Chen's (1985) solution by applying the similarity transformation defined in (29) and (30) to A_1 and B_1 with $\phi = 2.1805$ and $\theta = 11.048°$. These new values of A_1' and B_1' give a solution that compares well with the exact solution as shown in Fig. 9. Since any other values of ϕ and θ can be chosen, an infinite number of solutions for the angular variation of the displacements is possible when the eigenvalue λ is complex. With the above transformation the accuracy of the finite element solution compared to the exact solution defined by Chen (1985) is very high. Figure 10 provides results similar to those shown in Fig. 9, where the finite element solution is compared to $h'(\theta)$ and $-l'(\theta)$ instead of $f_j'(\theta)$ and $-g_j'(\theta)$. Here again the eigenvectors A_2 and B_2 obtained directly from the finite element solution appear different from the exact solutions. The same similarity transformation ($\phi = 2.1805$ and $\theta = 11.048°$) applied to A_2 and B_2 leads to values A_2' and B_2' that match the exact solution very closely.

Comparison of the stress singularities with existing analytical solutions

Yamada and Okumura (1983a) have shown the accuracy of the method for predicting the values of the order of the stress singularities in isotropic materials. The current section concentrates on the accuracy of predicting the values of the order of the stress singularities in anisotropic materials. The number of examples available in the literature which provide the exact values of the order of the stress singularities for different geometries is limited. Several simple cases have been considered and results from the current finite element method are compared.

The first case of interest is that of Delale *et al.* (1982), which considers the value of the order of the stress singularity at the apex of a cylindrically orthotropic wedge. Figure 11 shows a cylindrically orthotropic wedge of angle ψ, where the material properties given in the polar coordinate system are constant at every location in the wedge. The results are compared with the analytical solution of Delale *et al.* (1982) for their material referenced as 2 and whose relative properties are shown in Fig. 11. Table 3 compares results obtained using eqn (29) of Delale *et al.* (1982) and eqn (14) in the current paper. Note that for this particular case of cylindrical orthotropy, the property transformations expressed by equations (16–24) are not used. The results for the eigenvalue λ shown in Table 3 correspond to plane stress conditions which lead to the most severe stress state. The accuracy of the current method is very good with only 10 elements in the wedge. A slight decrease in

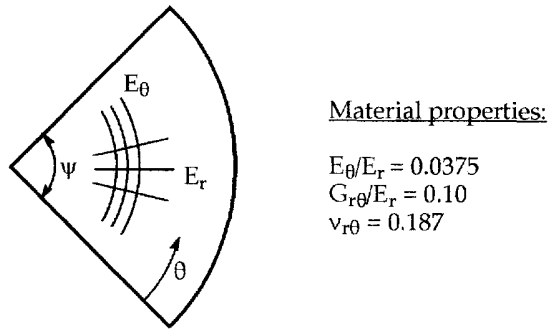

Fig. 11. Cylindrically orthotropic wedge of angle Ψ.

Table 3. Values of λ for a cylindrically orthotropic wedge of angle Ψ (Fig. 11)

Wedge angle Ψ (degrees)	10-element model	Exact value [Delale *et al.* (1982)]	Current λ / Exact λ
120	0.715154	0.714968	1.000260
180	0.310285	0.310184	1.000326
240	0.187098	0.187004	1.000503
300	0.150841	0.150754	1.000577
360	0.144508	0.144392	1.000803

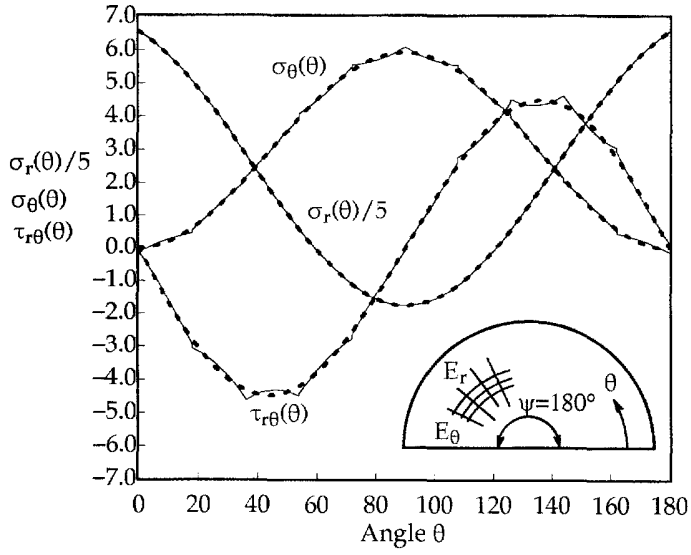

Fig. 12. Stress field for the case in Fig. 11 with Ψ = 180 . Analytical (dashed lines, Delale *et al.*, 1982) and FEM (10-element model) solutions.

accuracy occurs with increasing wedge angle ψ. Increasing the number of elements will improve the accuracy.

The accuracy of the angular variation of the displacement fields has been shown in several previous examples. Here the accuracy of the angular variation of the stress field is shown for the cylindrically orthotropic example shown in Fig. 11 with the wedge angle $\psi = 180°$. Using the analytical solution provided by eqns (17), (29) and (38) of Delale *et al.* (1982), exact results were computed corresponding to the most severe stress singularity, $\lambda = 0.310$. These stress fields are shown as the dashed lines in Fig. 12. Results obtained from the current formulation using a 10-element model are shown as solid lines. The radial stresses predicted by the two methods are essentially identical and the circumferential and shear stresses compare very well. Since the radial derivatives of the displacement field are

Table 4. Convergence of several eigenvalues λ_i for a cylindrically orthotropic wedge of angle $\Psi = 360^\circ$ (Fig. 11)

Eigenvalue	10-element model	20-element model	30-element model	Exact [Delale *et al.* (1982)]
λ_1	0.144508	0.144399	0.144393	0.144392
λ_2	0.165628	0.165037	0.165004	0.164994
λ_3	0.336346	0.334491	0.334386	0.334357
λ_4	0.547032	0.541935	0.541640	0.541559
λ_5	0.787123	0.774934	0.774212	0.774015

obtained analytically and the circumferential derivatives are obtained numerically from the shape functions, these differences are expected. Note that in this rather crude model, small discontinuities in shear and circumferential stresses exist at the nodes. These small discontinuities approach zero as more elements are used in the model. The difference between the exact and approximate stress distribution tends to average to zero over each element. These differences approach zero on a point by point basis as more elements are used in the model.

The case of cylindrical orthotropy treated here is interesting in the sense that an unusually high number of eigenvalues λ leading to a singular stress state can be found. This is shown in Table 4 for $\Psi = 360^\circ$ where the interface at $\theta = 0, 360^\circ$ represents a disbond. The current solution is compared to the exact solution for different numbers of elements in the model to show convergence trends when noncritical values of λ (i.e. not necessarily leading to the most severe stress state) are extracted from the current formulation. Note that the higher the number of eigenvalues needed, the more elements are needed to obtain the same level of accuracy as that of the most critical eigenvalue. The use of higher order eigenvalues is necessary when calculating stresses; see, for example, Kaya and Erdogan (1987). They show that convergence of the numerical solution to a class of singular integral equations is greatly improved by incorporating higher roots λ. Therefore, if the current solution is used in the development of a special element, it is clear that considering only the most critical root would lead to convergence problems because of the number and close proximity of other eigenvalues which lead to a singular stress state. With regard to a possible failure theory, a simple theory could make use of only the highest order singularity (Delale *et al.* 1982), but it is likely that a better theory can result from a more accurate solution to the stress field which requires more singular eigenvalues.

The case of orthotropic wedges as defined by Bogy (1972) is also of interest. The comparison of results obtained using Bogy's (1972) formulation and the current method has already been presented for different materials by Selvarathinam and Pageau (1994) and will not be repeated here. It can be seen there that the orders of singularity predicted by the two formulations are coincident to 0.05% accuracy in all cases considered using models with only 20 elements.

Presentation of new results

The simplicity and performance of the method is demonstrated for several different geometries and material properties for which analytical solutions would be tedious to obtain. The first case considered is shown in Fig. 13. Two half-planes with cylindrical orthotropic material properties are bonded together. The material properties of material 1 are held constant with relative values as indicated in the Figure, while the properties of material 2 are varied such that the ratios $E_{\theta 2}/E_{r2}$, $G_{r\theta 2}/E_{r2}$, and the value of $\nu_{r\theta 2}$ are held constant. The order of the stress singularity λ which results from the material discontinuity shown in Fig. 13 is plotted as a function of the ratio E_{r2}/E_{r1} in Fig. 14. These results were obtained using 10 elements for each half-plane. There are five values of λ which lead to a singular stress state throughout the range of material properties of material 2.

When the ratio E_{r2}/E_{r1} is very small, material 1 is almost a free–free half-plane with values of λ tending to the limiting values $\lambda_2 = 0.3102$ and $\lambda_4 = 0.7148$. Note that the first value can be retrieved with more significant digits from Table 3. As far as material 2 is concerned, and since material 1 appears very stiff in comparison to material 2, material 2

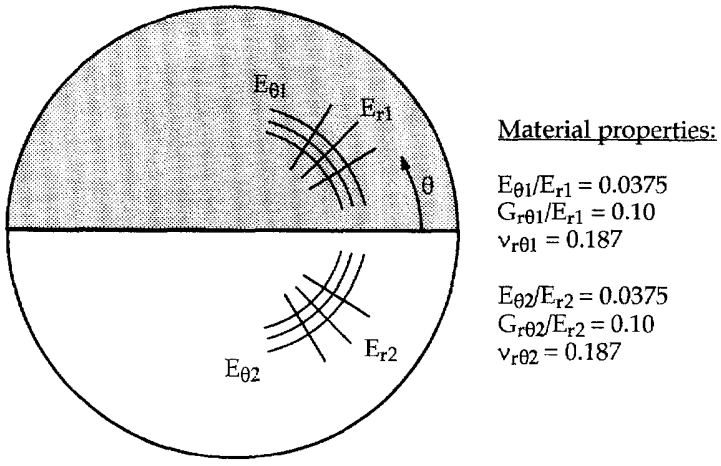

Fig. 13. Two bonded cylindrically orthotropic half-planes.

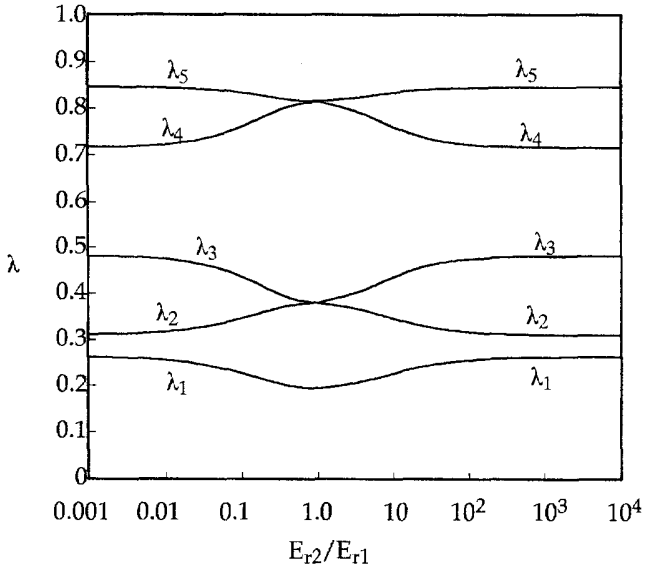

Fig. 14. Values of λ for two bonded half-planes with cylindrical orthotropy (Fig. 13).

is almost a clamped–clamped half-space with values of λ tending to the limiting values $\lambda_1 = 0.2619$, $\lambda_3 = 0.4809$ and $\lambda_5 = 0.8442$. When the ratio $E_{r2}/E_{r1} = 1.0$, the two materials are identical and the values of λ exhibit one single and two double roots as shown in the figure. When $(E_{r2}/E_{r1}) > 1$, the values of λ are the same as those obtained by considering the ratio $1/(E_{r2}/E_{r1})$ due to the geometrical symmetry of the problem with respect to the line bonding the two materials.

The second case considered is shown in Fig. 15. Two half-planes, one with cylindrical orthotropy and the other with rectangular orthotropy as shown in the figure, are bonded together. The material properties of material 1 are held constant with relative values as indicated in the figure, while the properties of material 2 are varied such that the ratios E_{y2}/E_{x2}, G_{xy2}/E_{x2}, and the value of v_{xy2} are held constant. The order of the stress singularity λ which results from the material discontinuity shown in Fig. 15 is plotted as a function of the ratio E_{x2}/E_{r1} in Fig. 16. These results are obtained using 10 elements for each half-plane. Figure 16 looks very different from Fig. 14. However, it is possible to distinguish some common features between the two figures. When the ratio E_{x2}/E_{r1} is very small, material 1 is almost a free–free half-plane with values of λ tending to the limiting values $\lambda_1 = 0.3102$ and $\lambda_2 = 0.7148$, that is, the same values as for Fig. 14. Material 2 is nearly a

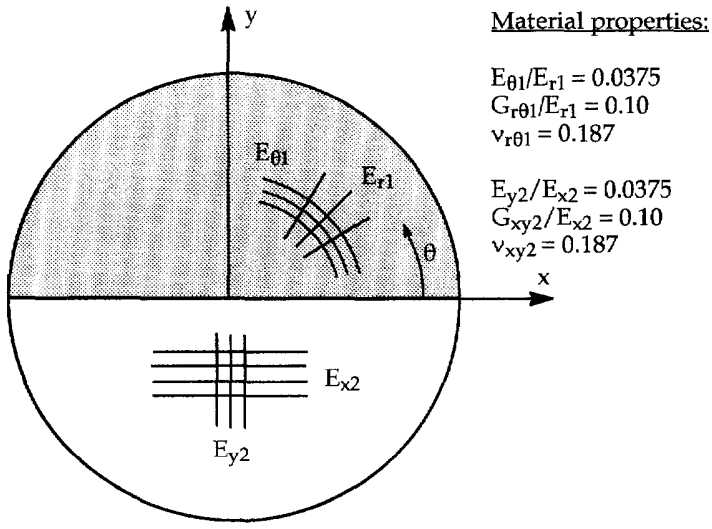

Fig. 15. Two bonded orthotropic half-planes.

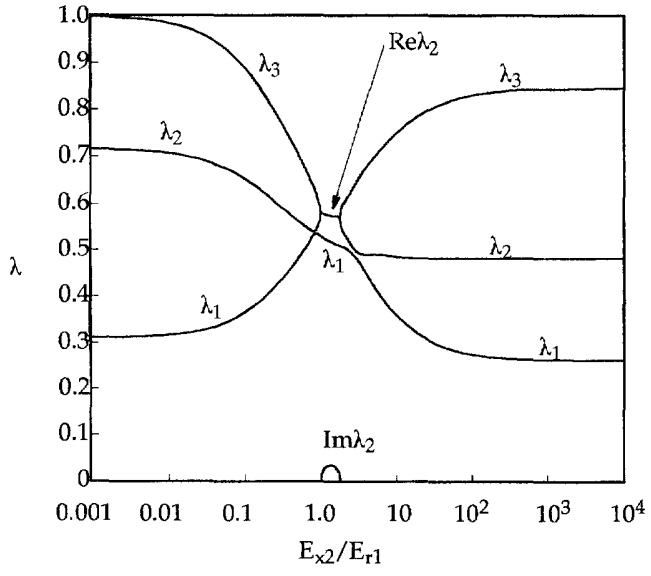

Fig. 16. Values of λ for two bonded half-planes (Fig. 15).

clamped–clamped half-plane with no singular point, and therefore there is no value λ between 0 and 1 for this half-plane. When the ratio E_{x2}/E_{r1} is very large, material 1 is nearly a clamped–clamped half-plane with values of λ tending to the limiting values $\lambda_1 = 0.2619$, $\lambda_2 = 0.4809$ and $\lambda_3 = 0.8442$, that is, the same values as for Fig. 14. Material 2 approaches a free–free half-plane with no singular point, and therefore there is no value λ between 0 and 1 for this half-plane. When the ratio E_{x2}/E_{r1} is close to unity, λ has one real value and one that is complex. Based on these results, if material 2 is bonded to material 1 in order to reduce the stress singularity, it seems better to have the properties of material 2 close to those of material 1 to maximize the values of λ (minimize the stress singularity).

The last two cases considered are directly obtained from those of Figs 13 and 15, as shown in Figs 17 and 19. The only difference is that a crack-like disbond has been introduced on half of the bond in the latter two cases. Figures 18 and 20 give the results for the values λ corresponding to problems of Figs 17 and 19, respectively. The results obtained for the bonded cases already given in Figs 14 and 16 are reproduced as dashed lines in Figs 18 and 20, respectively, for comparison.

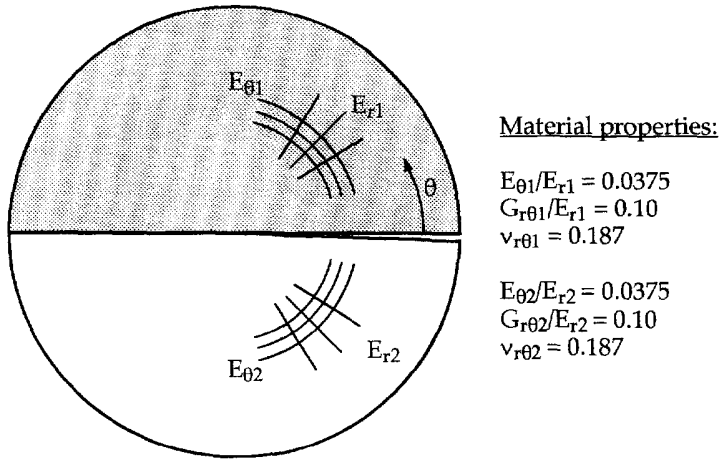

Fig. 17. Two disbonded cylindrically orthotropic half-planes.

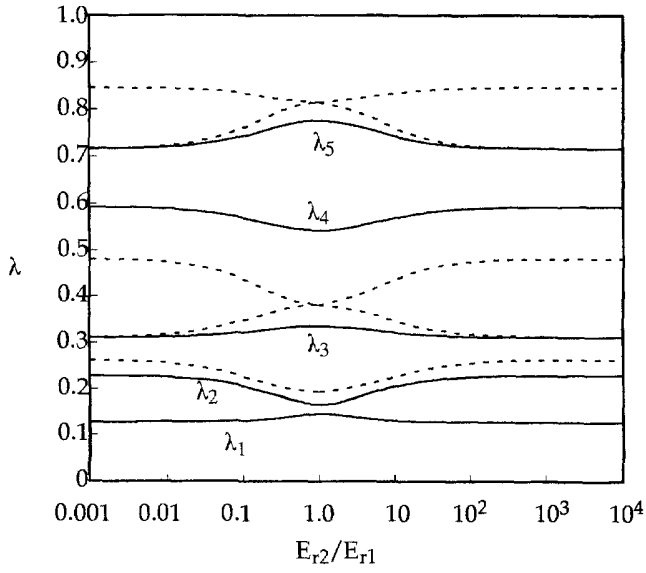

Fig. 18. Values of λ for two disbonded half-planes with cylindrical orthotropy (Fig. 17).

The results shown in Fig. 18 demonstrate that the shape of the curves representative of the different values λ are not greatly affected by the disbond. However, the values of λ are lower than those of Fig. 14, as expected. When the ratio E_{r2}/E_{r1} is very small, material 1 is almost a free–free half-plane with values of λ tending to the limiting values $\lambda_3 = 0.3102$ and $\lambda_5 = 0.7148$. Material 2 is almost a clamped–free half space with values of λ tending to the limiting values $\lambda_1 = 0.1262$, $\lambda_2 = 0.2281$ and $\lambda_4 = 0.5917$. When $(E_{r2}/E_{r1}) > 1$, the values of λ are the same as those obtained by considering the ratio $1/(E_{r2}/E_{r1})$, due to the geometrical symmetry of the problem with respect to the line bonding the two materials. Note that for the ratio $E_{r2}/E_{r1} = 1$, the values of λ can be found in Table 4 for 20 elements in the model.

The results shown in Fig. 20 are very different from those of Fig. 16. When the ratio E_{x2}/E_{r1} is less than 1, one of the three roots is complex. The complex root, whose real part tends to the limiting value 0.5 when the ratio E_{x2}/E_{r1} goes to zero, corresponds to material 2 being almost a clamped–free half-plane. Therefore, the complex value of λ_2 was expected for $E_{x2}/E_{r1} < 1$. The two other limiting values of λ, obtained when the ratio E_{x2}/E_{r1} goes to zero, are those corresponding to material 1 being a free–free half-plane. These values have already been shown in Figs 14, 16 and 18. When the ratio E_{x2}/E_{r1} is large, material 1 is

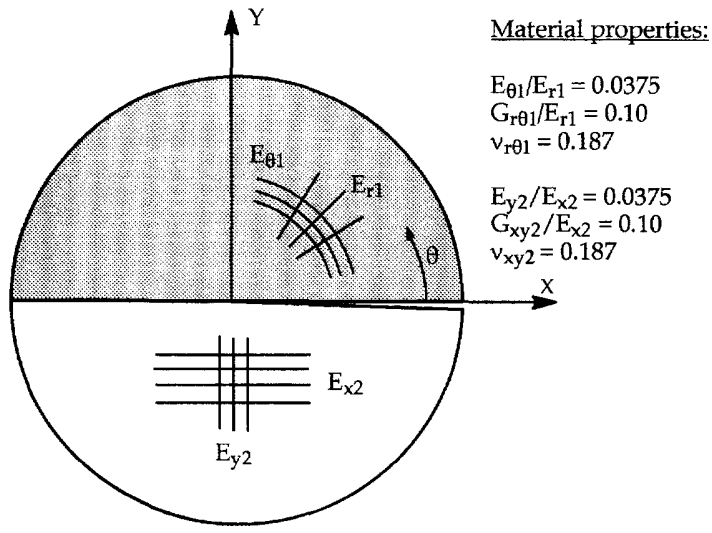

Fig. 19. Two disbonded orthotropic half-planes.

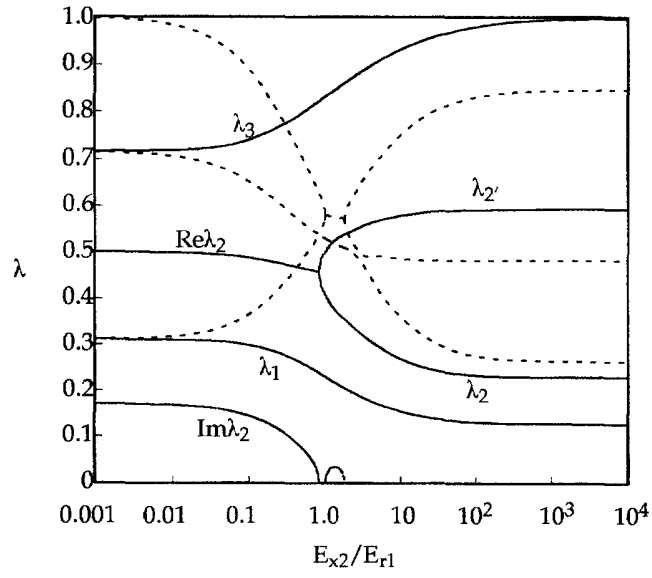

Fig. 20. Values of λ for two disbonded half-planes (Fig. 19).

almost a clamped–free half-plane for which $\lambda_1 = 0.1262$, $\lambda_2 = 0.2281$ and $\lambda_2' = 0.5917$, as previously seen in Fig. 18.

CONCLUSIONS

A finite element formulation has been developed for determining the order of the singularity and the angular variation of the inplane displacement and stress fields around a singular point in anisotropic materials. The sectorial element displacement shape functions are quadratic in the angular direction and exponential in the radial direction. Numerical integration is required only in the angular direction resulting in a very computationally efficient formulation. The rapid convergence of the element has been demonstrated by comparison to several available exact solutions. Low-order quadrature yields very accurate results when a reasonable number of elements is used. Monotonic convergence is observed with mesh refinement in isotropic materials and both monotonic or/and oscillatory convergence is observed with anisotropic materials. When the order of the stress singularity is

complex, it has been shown that the angular variation of the displacement and stress fields can be expressed in an infinite number of ways. It is possible to match previously published results with the current formulation by use of similarity transformations. These transformations have no influence on the actual displacement and stress fields, but they do influence the form of the field expressions. Predictions for both the order of singularity and the angular variation of the stress field in multi-material junctions have been shown to be accurate with very simple models. This accuracy and efficiency suggest that results from this approach could be used to formulate enriched elements for use in complex geometric configurations in anisotropic materials.

Acknowledgement—The first and third authors acknowledge the support of NASA Langley Research Center through grant NAG-1-1411. The second author acknowledges the support of the National Science Foundation through EPSCoR grant EHR-9108772.

REFERENCES

Barsoum, R. S. (1988a). Theoretical basis of the finite element iterative method for the eigenvalue problem in stationary cracks. *Int. J. Num. Meth. Engng* **26,** 531–539.

Barsoum, R. S. (1988b). Application of the finite element iterative method to the eigenvalue problem of a crack between dissimilar media. *Int. J. Num. Meth. Engng* **26,** 541–554.

Bazant, Z. P. and Estenssoro, L. F. (1979). Surface singularity and crack propagation. *Int. J. Solids Structures* **15,** 405–426.

Benthem, J. P. (1977). State of stress at the vertex of a quarter-infinite crack in a half-space. *Int. J. Solids Structures* **13,** 479–492.

Bogy, D. B. (1971). On the plane elastostatic problem of a loaded crack terminating at a material interface. *J. Appl. Mech.* **38,** 911–918.

Bogy, D. B. (1972). The plane solution for anisotropic elastic wedges under normal and shear loading. *J. Appl. Mech.* **39,** 1103–1109.

Chen, E. P. (1985). Finite element analysis of a bimaterial interface crack. *Theoretical Appl. Fracture Mech.* **3,** 257–262.

Delale, F., Erdogan, F. and Boduroglu, H. (1982). Stress singularities at the vertex of a cylindrically anisotropic wedge. *Int. J. Fract.* **19,** 247–256.

Gu, L. and Belytschko, T. (1994). A numerical study of stress singularities in a two-material wedge. *Int. J. Solids Structures* **31,** 865–889.

Hein, V. L., and Erdogan, F. (1971). Stress singularities in a two-material wedge. *Int. J. Fract. Mech.* **7,** 317–330.

Hoenig, A. (1982). Near tip behavior of a crack in a plane anisotropic elastic body. *Engng Fract. Mech.* **16,** 393–403.

Kaya, A. C., and Erdogan, F. (1987). On the solution of integral equations with a generalized Cauchy kernel. *Quart. Appl. Math.* **XLV**(3), 455–469.

Lin, K. Y. and Mar, J. W. (1976). Finite element analysis of stress intensity factors for cracks at a bimaterial interface. *Int. J. Fract.* **12,** 521–531.

Ma, C. C. and Hour, B. L. (1989). Analysis of dissimilar anisotropic wedges subjected to antiplane shear deformation. *Int. J. Solids Structures* **11,** 1295–1309.

Pageau, S. S., Joseph, P. F. and Biggers, S. B. Jr (1994a). The order of stress singularities for bonded and disbonded three material junctions. *Int. J. Solids Structures* **31,** 2979–2987.

Pageau, S. S., Joseph, P. F. and Biggers, S. B. Jr (1994b). A finite element analysis of the singular stress fields in anisotropic materials loaded in antiplane shear. *Int. J. Num. Meth. Engng* (in press).

Raju, I. S. and Crews, J. H. Jr (1981). Interlaminar stress singularities at a straight free edge in composite laminates. *Computers Structures* **14,** 21–28.

Selvarathinam, A. S. and Pageau, S. S. (1994). The order of stress singularities in orthotropic wedges. *J. Appl. Mech.* (submitted).

Sih, G. C., Paris, P. C. and Irwin, G. R. (1965). On cracks in rectilinearly anisotropic bodies. *Int. J. Fract. Mech.* **1,** 189–202.

Sukumar, N. and Kumosa, M. (1992). Application of the finite element iterative method to cracks and sharp notches in orthotropic media. *Int. J. Fract.* **58,** 177–192.

Yamada, Y., Ezawa, Y., Nishigushi, I. and Okabe, M. (1979). Reconsiderations on singularity or crack tip elements. *Int. J. Num. Meth. Engng* **14,** 1525–1544.

Yamada, Y. and Okumura, H. (1983a). Finite element analysis of stress and strain singularity eigenstate in inhomogeneous media or composite materials. In *Hybrid and Mixed Finite Methods* (Edited by Atluri, S. N., Gallagher, E. R. and Zienkiewicz, O. C.), pp. 325–343. John Wiley, New York.

Yamada, Y. and Okumura, H. (1983b). Analysis of local stress in composite materials by the 3-d finite element. In *Proc. Japan–U.S.A. Conference* (Edited by Kawata, K. and Akasaka, T.), pp. 55–64. Tokyo, 1981.